tvst

Glaucoma

The Effects of Negative Periocular Pressure on Biomechanics of the Optic Nerve Head and Cornea: A Computational Modeling Study

Babak N. Safa[1], Adam Bleeker[2], John P. Berdahl[3,4], and C. Ross Ethier[1]

[1] Wallace H. Coulter Department of Biomedical Engineering, Georgia Institute of Technology/Emory University, Atlanta, GA, USA
[2] Dean McGee Eye Institute Department of Ophthalmology, University of Oklahoma Health Sciences Center, Oklahoma City, OK, USA
[3] Equinox Ophthalmic, Newport Beach, CA, USA
[4] Vance Thompson Vision, Sioux Falls, SD, USA

Correspondence: C. Ross Ethier, Petit Biotechnology Building (IBB), 315 Ferst Drive, Room 2306, Atlanta, GA 30332-0363, USA. e-mail: ross.ethier@bme.gatech.edu

Received: May 19, 2022
Accepted: January 1, 2023
Published: February 6, 2023

Keywords: glaucoma; biomechanics; intraocular pressure (IOP); multi-pressure dial system; finite element method

Citation: Safa BN, Bleeker A, Berdahl JP, Ethier CR. The effects of negative periocular pressure on biomechanics of the optic nerve head and cornea: A computational modeling study. Transl Vis Sci Technol. 2023;12(2):5, https://doi.org/10.1167/tvst.12.2.5

Purpose: The purpose of this study was to evaluate the effects of negative periocular pressure (NPP), and concomitant intraocular pressure (IOP) lowering, on the biomechanics of the optic nerve head (ONH) and cornea.

Methods: We developed a validated finite element (FE) model of the eye to compute tissue biomechanical strains induced in response to NPP delivered using the Multi-Pressure Dial (MPD) system. The model was informed by clinical measurements of IOP lowering and was based on published tissue properties. We also conducted sensitivity analyses by changing pressure loads and tissue properties.

Results: Application of −7.9 mmHg NPP decreased strain magnitudes in the ONH by c. 50% whereas increasing corneal strain magnitudes by c. 25%. Comparatively, a similar increase in corneal strain was predicted to occur due to an increase in IOP of 4 mmHg. Sensitivity studies indicated that NPP lowers strain in the ONH by reducing IOP and that these effects persisted over a range of tissue stiffnesses and spatial distributions of NPP.

Conclusions: NPP is predicted to considerably decrease ONH strain magnitudes. It also increases corneal strain but to an extent expected to be clinically insignificant. Thus, using NPP to lower IOP and hence decrease ONH mechanical strain is likely biomechanically beneficial for patients with glaucoma.

Translational Relevance: This study provides the first description of how NPP affects ONH biomechanics and explains the underlying mechanism of ONH strain reduction. It complements current empirical knowledge about the MPD system and guides future studies of NPP as a treatment for glaucoma.

Introduction

Glaucoma is the leading cause of irreversible blindness worldwide and is frequently associated with elevated intraocular pressure (IOP).[1] The biomechanical response of certain ocular tissues is thought to play a significant role in glaucoma pathogenesis; specifically, elevated IOP causes supra-physiologic mechanical loading of the optic nerve head (ONH) tissues, that is, lamina cribrosa (LC) and prelaminar tissue (PLT), which has been hypothesized to contribute to retinal ganglion cell (RGC) axonal damage and subsequent vision loss.[2–4] Therefore, clinical treatment for glaucoma seeks to decrease IOP.[5] Although current treatments can manage elevated IOP, vision loss continues to progress in almost 45% of patients, despite treatment.[6,7] Further IOP lowering in patients with normal IOP who are progressing has been shown to slow progression, with most of these patients showing IOP acrophase at night.[8,9] However, safely lowing IOP in these patients has proven difficult as the most effective treatments also carry significant morbidity,[10] emphasizing the need for novel treatment options.

The Multi-Pressure Dial system (MPD; Equinox Ophthalmic, Inc., Newport Beach, CA) is a medical

device that lowers IOP noninvasively via application of negative periocular pressure (NPP).[11,12] The MPD system consists of a pair of goggles connected to a programmable vacuum pump delivering adjustable NPP. The IOP-lowering effect of MPD is transient and concurrent with the use of the goggles,[13] and the MPD's primary use case is in patients with glaucoma who are progressing despite medical management to lower IOP. Although experimentally undetected thus far, the negative pressure very likely increases globe volume. Consequently, IOP decreases as measured in experiments on a cadaveric model[14] and in living subjects,[13] as well as predicted via a lumped-parameter biomechanical model.[15] Of note, we here define IOP as the pressure inside the eye referenced to the atmosphere (not to goggle pressure), consistent with all other pressure measurements in the body.

Despite IOP lowering due to NPP, there is no information regarding the effects of NPP on ocular tissue biomechanics, notably the ONH and cornea. Thus, our objective was to evaluate the biomechanical effects of NPP using validated finite element (FE) modeling, a computational technique that allows efficient and flexible parametric investigation of the effects of mechanical loads on ocular tissues.[16–22] We focused on the ONH because it is an early and important site of neurological damage in glaucoma, and decreased ONH strain is likely beneficial for the treatment of glaucoma, whereas increased strain of the ONH could be detrimental.[3,23,24] Secondarily, we explored mechanical strains in the cornea induced by NPP, which is directly loaded by the application of NPP.

Methods

We quantified the effects of NPP by simulating the biomechanical behavior of a human eye in several situations. We provide an overview of the simulations here, followed by full details below.

1. *Normotensive case:* A normal eye with an IOP of 15.8 mmHg.
2. *Goggle case:* The eye in case 1, acted on by NPP distributed over the cornea and limbal region, decreasing gradually toward the posterior pole. IOP was reduced concomitantly, as is experimentally observed to occur during goggle wear.[13]
3. *Hypertensive case:* The eye in case 1, except that IOP was doubled to 31.6 mmHg.
4. *IOP fixed case:* Similar to case 2, except that IOP was held constant at the normotensive level. Although it is known that IOP is lowered by NPP, this case is useful for understanding the mechanism by which NPP affects ONH biomechanics.

The biomechanical properties (stiffnesses) of ocular tissues were based on literature values, with adjustment to ensure that the modeled eye matched population-averaged ocular compliance data. We used ocular compliance for validation because it is a relatively well-characterized descriptor of corneoscleral shell biomechanical behavior, which in turn is expected to strongly influences how NPP will affect tissue strains within ocular tissues.

Tissue mechanical properties vary from one person to the next, so the biomechanical response due to NPP will vary from one person to the next. We, therefore, conducted a simplified sensitivity analysis to investigate the effects of such physiological variability. More complete sensitivity analyses are possible,[17,21] but were beyond the scope of this initial study.

Ocular Geometry and FE Modeling Technical Details

Our finite element model was based on existing FE models of the human eye,[17,22] with additional model dimensions obtained from the literature (Table 1). Following previous approaches,[25,26] we assumed axisymmetry to allow more rapid computations, considering a 5 degree "wedge" rather than an entire globe (Fig. 1). We modeled the rectus muscles/tendons as a rigid body at the superior aspect of the globe, obliquely attached to the sclera (see Fig. 1), with the insertion site placed c. 6 mm posterior to the limbus, spanning approximately 1 mm.[27]

This geometry was meshed with conforming second-order tetrahedral elements (TET10) in Gmsh (version 4.8.4)[28] using the "Frontal" algorithm.[29] Following initial mesh generation, 10 smoothing steps and 10 mesh optimization steps were performed, and the mesh was then exported as a version 2 "msh" file (ASCII). Based on a preliminary mesh sensitivity

Table 1. Summary of Key Dimensions for the Eye Model

	Value (mm)	Source
Corneal radius	7.80	26,61
Corneal thickness	0.56	26,62
Scleral radius	11.00	22,61
Scleral thickness	0.80	17,22
Retinal thickness	0.20	17,22
LC thickness	0.20	17,22

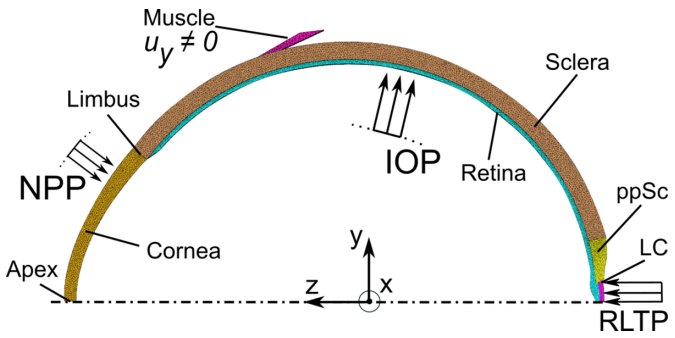

Figure 1. The finite element model used in this study, including the corneoscleral shell and ONH (ppSC = peripapillary sclera and LC = lamina cribrosa). The extraocular rectus muscle attachment is also shown, which is modeled as a rigid body free to move along the y-axis. The figure also schematically represents the loads, namely intraocular pressure (IOP), negative periocular pressure (NPP), and retrolaminar tissue pressure (RTLP).

analysis, we used 446,528 elements (element size factor c. 25–100 µm) to tesselate the domain, with elemental density enhanced 4-fold in the ONH.

All FE simulations were carried out using FEBio version 3.5.1.[30] We enforced axisymmetry through the appropriate specification of nodal degrees of freedom. Specifically, nodes on the axis of symmetry lying within the cornea, retina, and LC were constrained to move along the z-axis, whereas nodes on the bounding planes of the wedge were constrained to move in-plane, so their displacement was radial relative to the axis of symmetry (see Fig. 1). The muscle was free to move along the y-axis ($u_y \neq 0$), but was constrained in the remaining 5 degrees of freedom (see Fig. 1). To check the impact of this boundary condition, we mimicked a hinge-like muscle connection by allowing the muscle/tendon to also rotate around the x-axis (see Supplementary Fig. S1); however, this modification did not result in any significant change in the mechanical response of the model, and thus, for simplicity, we returned to the original boundary condition (only y-displacements allowed).

Specification of Ocular Pressures

Normotensive Case

This case describes a normal eye without goggles with the following loads typical for a healthy eye: IOP = 15.8 mmHg, NPP = 0, and retrolaminar pressure (RLTP) = 8 mmHg.[14] IOP was uniformly applied on the interior surface of the corneoscleral shell (see Fig. 1).

Goggle Case

To test the effects of NPP, we modeled a normotensive eye with MPD goggles applied, specifying the following pressures: IOP = 11.5 mmHg, NPP = −7.9 mmHg, and RLTP = 8 mmHg. NPP and IOP were based on experimental measurements,[13] where it was observed that imposing an NPP equal to 50% of the baseline IOP (here, NPP = −7.9 mmHg) reduced IOP to 11.5 mmHg. The NPP was applied uniformly from the corneal apex to 2.7 mm posterior to the limbus along the z-axis (see Fig. 1), then decreasing linearly to zero near the edge of the peripapillary sclera (ppSC). Unfortunately, there are no experimental data regarding the spatial distribution of NPP; therefore, to assess the effect of uncertainty in the spatial distribution of NPP, we also varied the distribution of NPP on the globe surface (see Supplementary Fig. S4), which showed no significant difference in results.

Hypertensive Case

We simulated the effects of elevated IOP (31.6 mmHg), with all other inputs being the same as in the Normotensive case. This allowed us to compare strains observed in the Goggle case to those occurring in ocular hypertension.

IOP Fixed Case

NPP both lowers IOP and expands the corneoscleral shell, which could be expected to have opposite effects on strains in the ONH.[25] Thus, to investigate the effects of only NPP-induced corneoscleral shell expansion on ONH biomechanics, we held IOP fixed at 15.8 mmHg while imposing NPP. This would likely not occur clinically but provides a useful mechanistic understanding of the effects of NPP on the eye's biomechanics.

Specification of Tissue Biomechanical Properties

To investigate the effects of tissue stiffness, we considered a range of tissue mechanical properties, which we refer to as tissue parameter sets. In all cases, except those noted explicitly below, we used a nearly incompressible neo-Hookean hyperelastic solid constitutive formulation to describe the mechanical behavior of tissues, where Young's modulus E was the model parameter (for details of constitutive equation see Appendix). The neo-Hookean constitutive formulation demonstrates nearly linear mechanical behavior, which is appropriate in view of the small deformations in our simulations. In addition, for simplicity, we did not consider pre-strain/stress in our model; however, all the comparisons to assess NPP's effect in this study were made relative to the Normotensive case. Making all comparisons relative to the Normotensive case, together with the near-linear behavior of the consti-

tutive model, minimize the impact of neglecting pre-strain/stress in our model.

In the *Baseline tissue parameter set*, values of E were based on literature reports, with modest adjustments to match clinical ocular compliance data (Table 2). To account for the microarchitecture of the ppSC, we included circumferential (along the x-axis; see Fig. 1) collagen fibers in the ppSC, described by a 1-D linear elastic constitutive relation, with fiber modulus value (E_f = 41.83 MPa).[31] When modeling fibers, we did not consider the effect of fiber distribution and crimp, which effectively corresponds to an upper bound on ppSC stiffness. Last, as a diagnostic test case, we considered the effects of reducing ppSC stiffness by eliminating collagen fibers from the ppSC, similar to Sigal et al.[22,25] This corresponds to a lower bound for ppSC stiffness and produced results in agreement with the previous work by Sigal et al. (Supplementary Fig. S3).

Soft and Stiff (Corneoscleral) Shell Tissue Parameter Sets

We investigated the effects of corneoscleral shell stiffness by doubling or halving sclera, ppSC, and cornea matrix stiffnesses, denoted as *Stiff Shell* and *Soft Shell tissue parameter sets*, respectively (see Table 2). This range of variation was inspired by the reported range of values for the human eye's mechanical properties.[22,32–34]

Table 2. Summary of Tissue Biomechanical Stiffnesses (E, in MPa) used in Simulations, With Corresponding Literature Reference

	Tissue Parameter Sets		
Tissue	Baseline	Soft Shell/ Stiff Shell	Soft LC/ Stiff LC
Sclera	4.50[22,*]	2.25/9	Same
ppSC matrix	4.50[22,*]	2.25/9	Same
ppSC fibers	41.83[31]	20.92/83.66	Same
LC	0.30[22]	Same	0.0026/3
Retina	0.06[17]	Same	Same
Cornea	0.84[33]	0.42/1.68	Same

In all simulations, the rectus muscle/tendon was treated as rigid. "Same" indicates that the values are the same as those listed for the *Baseline tissue parameter set*. *We multiplied the Young's modulus in Sigal et al.[22] by a factor of 1.5 to match the model's ocular compliance to the experimental values (see the text for further details).

Soft and Stiff LC Tissue Parameter Sets

We also studied the effect of varying the stiffness of the LC. In the *Stiff LC tissue parameter set*, we set the stiffness of the LC to be similar to scleral stiffness (E = 3 MPa), which represents a (non-physiological) limiting high-stiffness case, useful for sensitivity analysis (see Table 2). The *Soft LC tissue parameter set* was informed by ex vivo biomechanical measurements of the LC.[35] Specifically, we modeled the LC as a compressible neo-Hookean material with E = 2.6 kPa and Poisson's ratio ν = 0.23 following a well-established formulation.[36]

Model Validation

To validate the FE model, we compared our model's ocular compliance to literature values. Specifically, we computed the compliance of the corneoscleral shell in the Normotensive case as ϕ = d(IOV)/d(IOP), where d(IOV) is the change in intraocular volume (i.e., the volume enclosed within the corneoscleral shell; see Fig. 1, in response to a change in IOP, d(IOP)). The computed value of ϕ was compared to previous values summarized from multiple in vivo experiments[37] (Table 3), using the formula of McEwen and Helen: $\phi = (a \times \text{IOP} + b)^{-1}$, where a = 0.015 − 0.027 μL^{-1}, and b = 0.03 − 0.31 mmHg/μL evaluated at an IOP of 15 mmHg. To match compliance values in the literature, we increased the stiffness of the sclera, cornea, and ppSC matrix used by Sigal et al.[22] by a factor of 1.5 (see Table 2).

Modeling Outcomes and Data Analysis

Our primary outcome measures were the nodal distribution of the first and third principal Lagrangian strain (E_{I} and E_{III}, respectively), two standard measures of tissue deformation, representing maximal tensile (E_{I}) and compressive (E_{III}) strains in an isochoric deformation. Note that due to the compressibility of the LC in the soft LC parameter set, negative E_I values occurred, which were visualized using a value-preserving bi-symmetric logarithmic transformation.[38,39]

We considered strains in four tissue regions of interest: the LC (1643 LC nodes on the x = 0 plane), the prelaminar tissue (2357 PLT nodes on the x = 0 planes), the limbus (240 nodes shared by the cornea and sclera in 3D), and the corneal apex (440 corneal nodes on the x = 0 plane; see Fig. 1). More specifically, the PLT was defined as tissue within the retina having a radial distance from the axis of symmetry less than the LC radius in the x-y plane. The corneal apex was defined as the corneal region centered on the

symmetry plane having a diameter of 3.06 mm, which matches the region that would be directly applanated during Goldmann tonometry,[40] a region that is clinically familiar to practitioners. Finally, we evaluated the uniformity of the spatial placement of the selected nodes to avoid bias due to potential nodal clustering, confirming the appropriateness of our sampling (see Supplementary Fig. S2).

To make comparisons, we used the summary of strain values (median [interquartile range]) within each region. Due to the deterministic nature of computational studies, and the fact that the summary statistics were calculated using the same sampling points (i.e., nodes) for all the cases, statistical hypothesis testing was not suitable and was not carried out.

Results

Model Validation

We expected the eye's biomechanical response to NPP to depend strongly on volume increase in the corneoscleral shell, which can be macroscopically characterized by ocular compliance, ϕ. It was, therefore, important to validate our model against the values of ϕ provided in the literature. The compliance of our model in the Normotensive case was $\phi =$ 3.1 µL/mmHg, which is within the range of reported values for the human eye from in vivo experiments (ϕ = 1.4 − 3.9 µL/mmHg[37]).

Effects of NPP

Normotensive Case Versus Goggle Case

It was of interest to probe the strains in the LC, PLT, limbus, and at the corneal apex due to NPP in a normotensive eye (i.e., comparison between the Normotensive and Goggle cases). Using the *Baseline tissue parameter set*, NPP caused the median E_I, a measure of tissue tension, to decrease by 53.9% in the LC, from 0.52% [0.40% to 0.73%] (median [interquartile range]; Figs. 2A, 2M) to 0.24% [0.18% to 0.34%] (see Figs. 2D, 2M). Similarly, in the PLT, E_I decreased by 55.3%, from 0.92% [0.78% to 1.13%] (see Fig. 2A and 2M) to 0.41% [0.35% to 0.50%] (see Figs. 2D, 2M). Conversely, E_I at the limbus increased by 23.7%, from 0.69% [0.67% to 0.71%] (see Figs. 2B, 2M) to 0.86% [0.83%, 0.88%] (see Figs. 2E, 2M), and at the corneal apex by 25.3%, from 0.95% [0.74% to 1.20%] (see Figs. 2C, 2M) to 1.19% [0.94% to 1.48%] (see Figs. 2F, 2M).

Similarly, NPP caused the magnitude of $E_{III,}$, a measure of tissue compression, to decrease in the LC by 52.8%, with the value of E_{III} changing from −0.79% [−1.06% to −0.56%] (see Figs. 3A, 3M) to −0.37% [−0.50% to −0.25%] (see Figs. 3D, 3M), whereas in the PLT the magnitude of E_{III} decreased by 54.4%, with the value of E_{III} changing from −0.68% [−0.93% to −0.52] (see Figs. 3A, 3M) to −0.31% [−0.43% to −0.24] (see Figs. 3D, 3M). Contrary to the LC and PLT, NPP caused the magnitude of E_{III} at the limbus to increase by 24.2%, with E_{III} changing from −0.86% [−0.98% to −0.79%] (see Figs. 3B, 3M) to −1.07% [−1.21% to −0.97%] (see Figs. 3E, 3M), and at the corneal apex by 24.8%, with E_{III} changing from −1.78% [−2.20% to −1.41%] (see Figs. 3C, 3M) to −2.22% [−2.71% to −1.78%] (see Figs. 3F, 3M).

Hypertensive Case

In the Hypertensive case, where IOP was set to 31.6 mmHg and no goggles were present, the median E_I was significantly higher in the LC and PLT relative to the Normotensive case (201.2% and 184.0% greater in the LC and PLT, respectively, using the *Baseline tissue parameter set*; see Figs. 2G, 2M). Similarly, median E_I was 101.4% and 115.9% greater in the limbus and at the corneal apex, respectively (compared to the Normotensive case; see Figs. 2H, 2I, 2M). We note that the strain increases in the cornea due to ocular hypertension were almost 4 times larger than the 25% strain increases observed in the Goggle case (all referenced to the Normotensive case). Similarly, the magnitude of E_{III} increased by 190.9% and 180.1% in the LC and PLT, respectively (compared to the Normotensive case; see Figs. 3G, 3M). In addition, the magnitude of E_{III} increased by 101.0% at the limbus, and by 111.3% at the corneal apex (see Figs. 3H, 3I, 3M, using the *Baseline tissue parameter set*), which were again approximately 4 times larger than the 25% corneal strain increases observed in the Goggle case.

IOP Fixed Case

In this case, the IOP was artificially held constant when NPP was applied. We observed that NPP had minimal effects on E_I and E_{III} magnitudes in the LC and PLT, with a difference of less than 1% compared to the Normotensive case (see Figs. 2J-L, 2M and 3J-L, 3M). However, fixing the IOP led to a large increase in E_I in the cornea; specifically, at the limbus, E_I increased by 51.2% (see Fig. 2K), and at the corneal apex it increased by 56.1% (see Fig. 2I), all referenced to the Normotensive case. Similarly, the magnitude of E_{III} at the limbus increased by 51.5% (see Fig. 3K), and by 54.5% at the corneal apex (see Fig. 3I). In every instance, these corneal strain increases relative to the Normotensive case were much larger than those observed in the Goggle case.

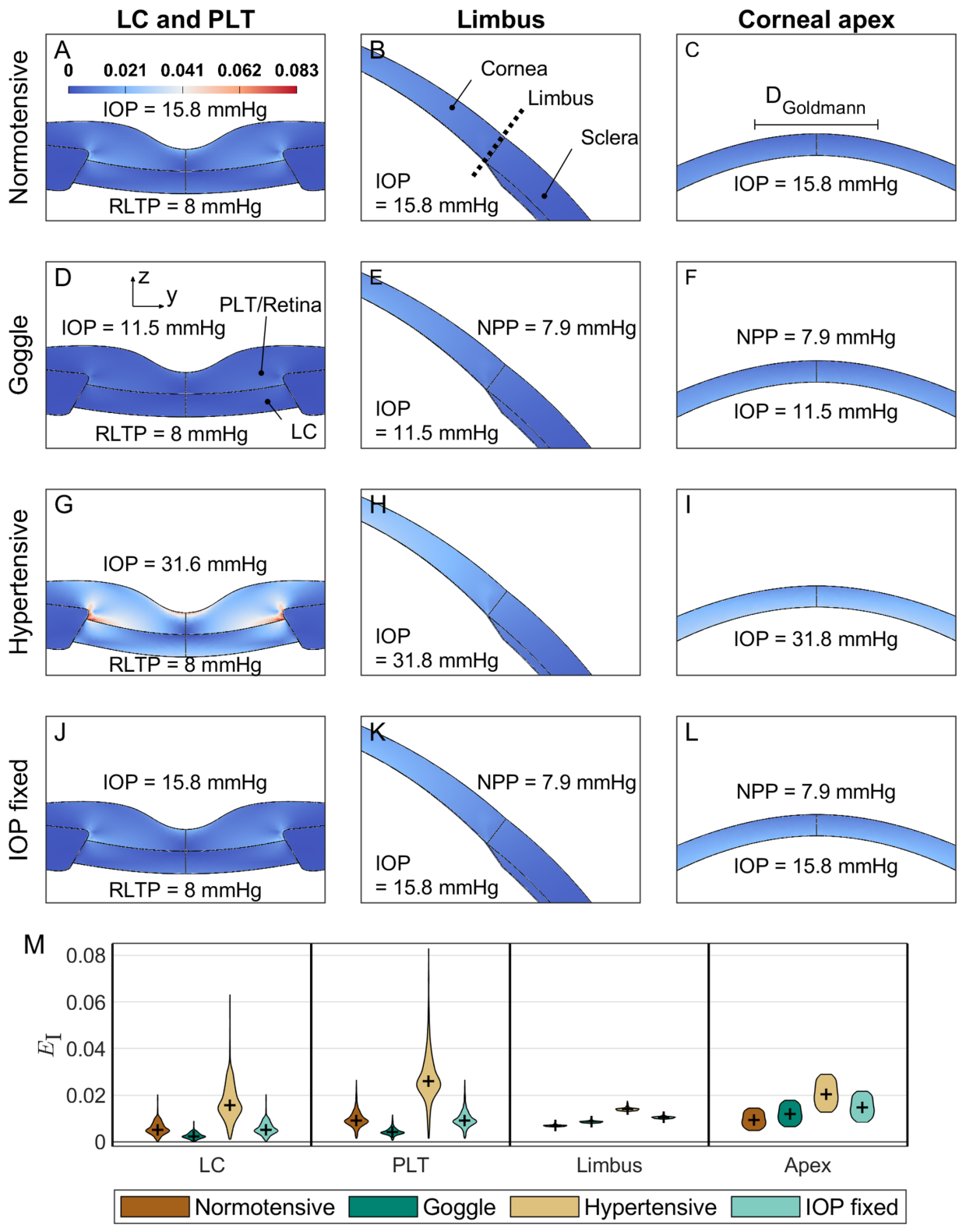

Figure 2. (**A-L**) Maps of the first principal Lagrangian strain (E_I), a measure of tissue stretching, in the LC, PLT, limbus, and at the corneal apex for tissue stiffnesses defined by the *Baseline tissue parameter set*. Each of the *top four rows* correspond to one case (i.e., Normotensive [**A-C**], Goggle [**D-F**], Hypertensive [**G-I**], and IOP fixed [**J-L**]). The *bottom row* (**M**) provides a summary of E_I values (violin plots [Bechtold, Bastian, 2016. Violin Plots for Matlab, Github Project, https://github.com/bastibe/Violinplot-Matlab, doi:10.5281/zenodo.4559847], with median shown by "+") in each region. $D_{Goldmann} = 3.06$ mm is the diameter of the applanated region during Goldmann tonometry, which is a clinically familiar region that we used to define the corneal apex region.

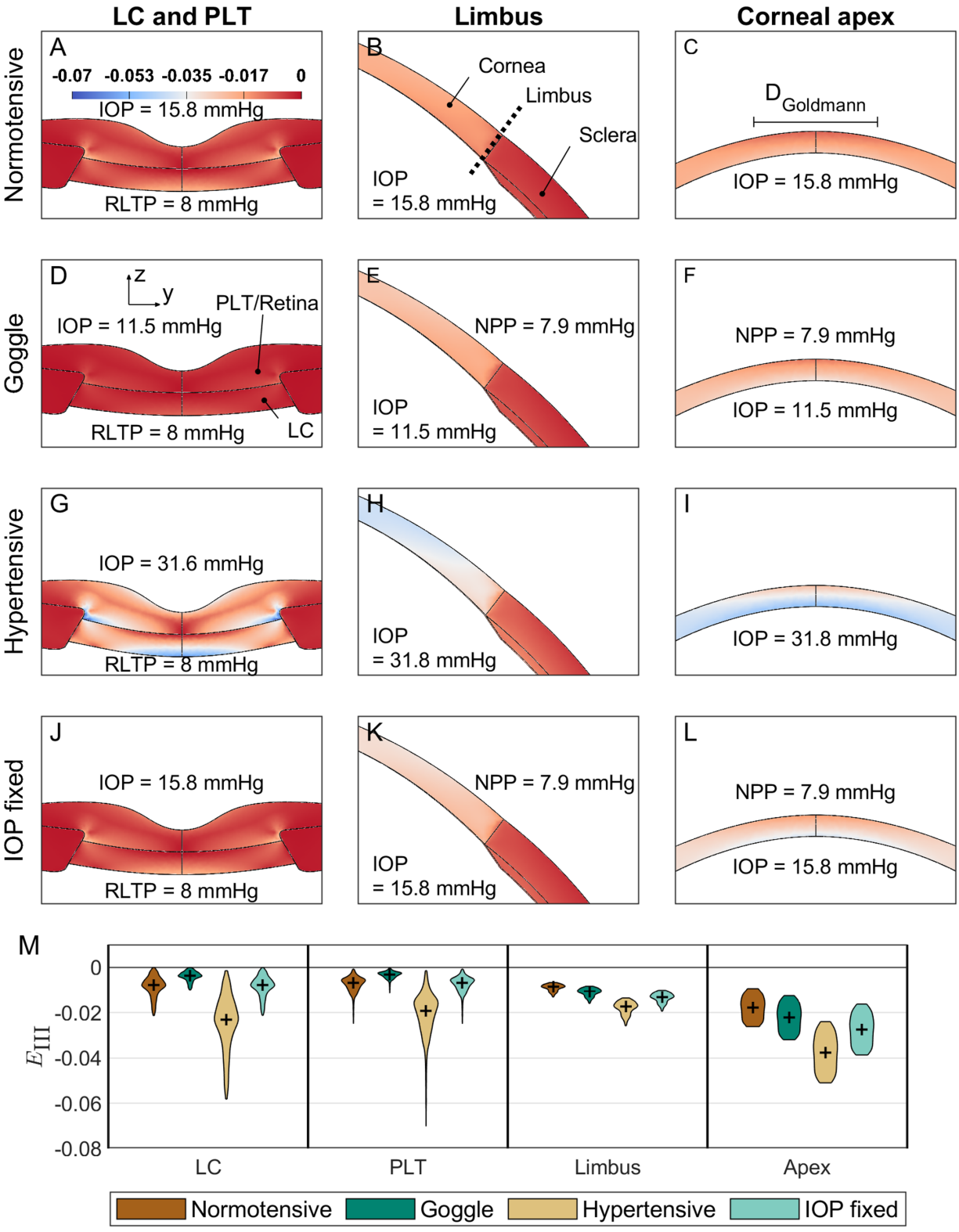

Figure 3. (**A-L**) Maps of the third principal Lagrangian strain (E_{III}), and (**M**) summary of E_{III} values for tissue stiffnesses defined by the *Baseline tissue parameter set*. For a detailed description of each panel see the caption of Figure 2.

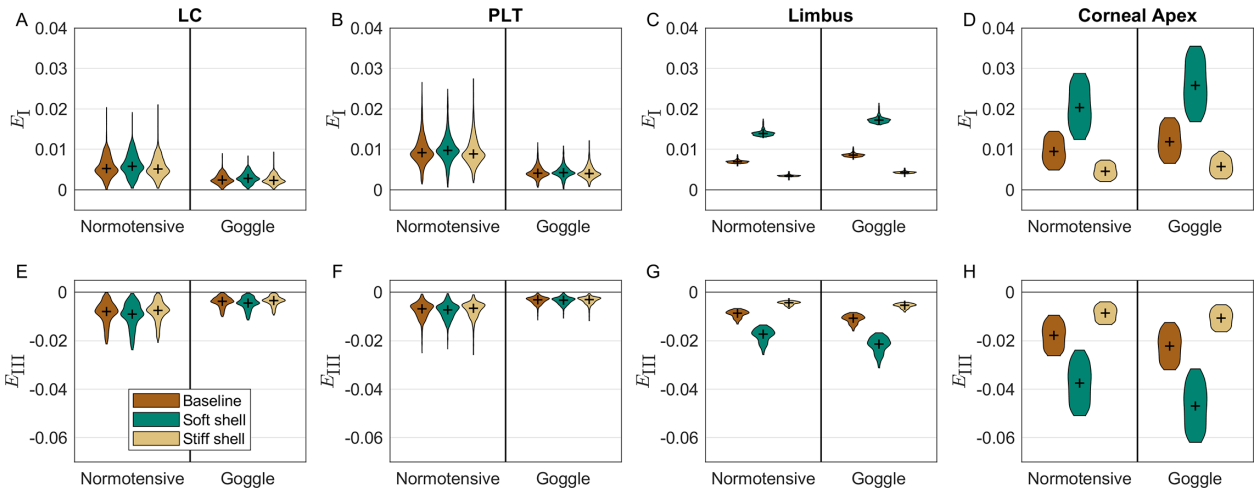

Figure 4. Changes in first (E_I) and third (E_{III}) principal strains due to varying corneoscleral shell stiffness. Calculations were carried out for both the Normotensive and Goggle cases, using the *Baseline*, *Soft Shell*, and *Stiff Shell tissue parameter sets* (Table 2). Each panel depicts the strain values in the Normotensive and Goggle cases in different tissues (lamina cribrosa [LC; **A** and **E**], prelaminar tissue [PLT; **B** and **F**], limbus [**C** and **G**], and corneal apex [**D** and **H**]). Changing corneoscleral shell stiffness did not change the effect of NPP in decreasing strain magnitudes in the lamina cribrosa (LC; **A** and **E**) and prelaminar tissue (PLT; **B** and **F**); however, softening (stiffening) corneoscleral shell stiffness increased (decreased) E_I and E_{III} magnitudes at the limbus (**C** and **H**) and corneal apex (**D** and **H**). Data is shown using violin plots, with the median shown by "+."

Sensitivity of Tissue Strains to Stiffness Modulation

Soft and Stiff Shell Tissue Parameter Set

Changing corneoscleral shell stiffness within a physiological range using the *Soft/Stiff Shell tissue parameter sets* (see Table 2) had only a small effect on strain magnitudes in the LC and PLT. More specifically, relative to the Normotensive and Goggle cases that were modeled using the *Baseline tissue parameter set* of tissue properties, softening the shell caused an overall increase of 3.4% to 16.0% in LC and PLT strain magnitudes, whereas stiffening the corneoscleral shell caused less than 5% change in strain magnitudes (Figs. 4A, 4B, 4E, 4F). In contrast, the strains at the limbus and corneal apex approximately doubled using the *Soft Shell tissue parameter set* and halved for the *Stiff Shell tissue parameter set* compared to results obtained with the *Baseline tissue parameter set* for both the Normotensive and Goggle cases (see Figs. 4C, 4D, 4G, 4H). Importantly, the decrease in ONH strains and increase in corneal strains seen in the Goggle case relative to the Normotensive case persisted when using the *Soft/Stiff Shell tissue parameter sets* to describe tissue stiffnesses (see Fig. 4).

Soft and Stiff LC Tissue Parameter Sets

As expected, significantly lowering the LC stiffness, and adding compressibility to mimic the ex vivo properties of the ONH (*Soft LC tissue parameter set*; see Table 2) markedly increased strain magnitudes in the LC and PLT (Figs. 5A, 5C). Specifically, in the Normotensive case simulated using the *Soft LC tissue parameter set*, E_I of the LC increased by a factor of 6.1 relative to the Normotensive case simulated with the *Baseline tissue parameter set*, where E_I increased by a factor of 2.8 in the PLT as a result of using *Soft LC tissue parameter set* (see Fig. 5A). Similarly, in the Goggle case, when using the *Soft LC tissue parameter set*, E_I was greater by a factor of 5.7 in the LC and 2.9 in the PLT as compared to the *Baseline tissue parameter set* (see Fig. 5C). Further, the magnitude of E_{III} was greater by a factor of 31.9 in the LC and 3.6 in the PLT in the Normotensive case, and by a factor of 64.9 in LC and 3.6 in the PLT in the Goggle case (see Figs. 5A, 5C), again compared to using the *Baseline tissue parameter set*. Conversely, stiffening the LC (using the *Stiff LC tissue parameter set*; see Table 2), so that the LC stiffness was similar to that of the sclera, decreased E_I and the magnitude of E_{III} in both the LC and PLT by c. 75% (see Fig. 5).

Interestingly, the observation that E_I and E_{III} magnitudes in the LC and PLT were lower in the Goggle case relative to the Normotensive case was largely unaffected by changing the stiffness and compressibility of the LC. The exception was for the values of E_{III} in the LC for the *Soft LC tissue parameter set*, where only a 3.9% decrease in LC E_{III} magnitude was observed due to the goggles compared to the Normotensive case (see Fig. 5C).

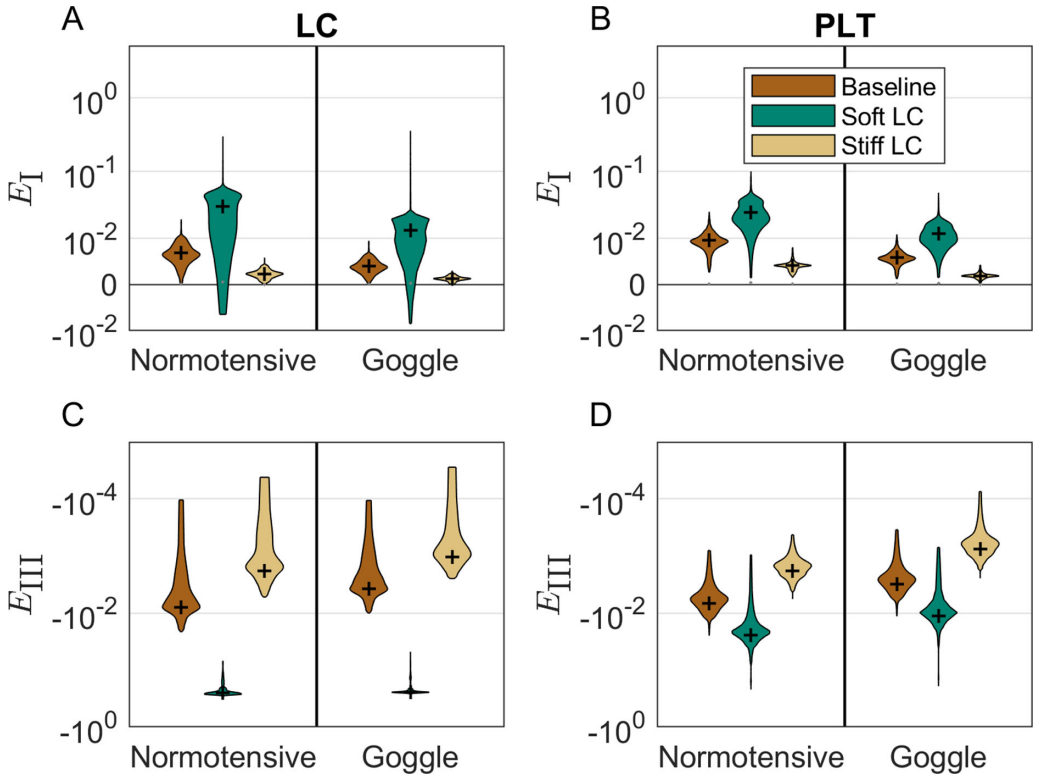

Figure 5. The effects of changing LC stiffness on strains (E_I and E_{III}) in the lamina cribrosa [LC; **A** and **C**] and prelaminar tissue [PLT; **B** and **D**]) using Baseline, Soft LC, and *Stiff LC tissue parameter sets* (Table 2). The magnitudes of E_I and E_{III} increased in both the LC (**A** and **B**) and the PLT (**C** and **D**) when using *Soft LC tissue parameter set* relative to the values computed when using the *Baseline tissue parameter set*. Conversely, when using the *Stiff LC tissue parameter set*, they decreased. However, despite these changes, for both the *Soft and Stiff LC tissue parameter sets*, the magnitudes of E_I and E_{III} decreased in the Goggle case relative to the Normotensive case. Data is shown using violin plots and the median is marked with "+."

Discussion

This study evaluated the biomechanical response of the optic nerve head (ONH) and cornea to negative periocular pressure (NPP). Our results indicate that NPP significantly decreases mechanical strain in the ONH while increasing it in the cornea (see Figs. 2, 3). This effect occurred over a wide range of tissue stiffnesses. Consistent with the known benefit of lowering IOP, and the understanding of the role of ONH biomechanics in glaucoma, reducing ONH biomechanical strain is predicted to slow or stop retinal ganglion cell axonal damage. Several clinical studies have established the association between glaucoma and IOP,[41,42] where, for instance, the Early Manifest Glaucoma Trial demonstrated that every 1 mmHg decrease in IOP is associated with a 10% decrease in glaucomatous progression.[6] Although the exact mechanism by which IOP lowering slows glaucomatous progression is unknown, it is widely hypothesized that this protective effect is due to reduced mechanical strains within the lamina cribrosa.[2,43,44] The reduction in ONH strain due to NPP is thus predicted to be beneficial for patients with glaucoma.

The decrease in the ONH strains was not sensitive to changing the corneoscleral shell stiffness (LC, Figs. 4A, 4E; PLT Figs. 4B, 4F), nor was it sensitive to changing the spatial distribution of NPP (see Supplementary Fig. S4), suggesting that the decrease in IOP due to NPP is the primary cause of the decrease in the ONH strains (Figs. 2, 3). This is also consistent with the outcome of the IOP fixed case, in which globe expansion without IOP lowering did not reduce ONH strains. This result was non-obvious because NPP both lowers IOP (expected to reduce ONH strain) and expands the corneoscleral shell (expected to increase ONH strain); it appears that for the range of tissue stiffnesses that we considered, the IOP decrease effect dominates any expansion of the corneoscleral shell.

The insensitivity of computed strains in the LC and PLT to a change in corneoscleral shell stiffness was due to including ppSC fibers in our model because these are important determinants of ppSC deformations and hence scleral canal expansion during globe volume changes. In fact, when collagen fiber-reinforcement in

the ppSC was eliminated, ONH strains were sensitive to changing corneoscleral shell stiffness (see Supplementary Fig. S3), consistent with the findings of Sigal et al., in which ppSC fibers were not considered.[25] Nevertheless, independent of whether ppSC collagen fibers were modeled or not, NPP decreased ONH strains, further supporting the strain-reducing effect of NPP on the ONH.

Interestingly, the biomechanical properties of the LC, and especially its compressibility, showed a significant effect on the strain-reducing effect of NPP in ONH (see Fig. 5). More specifically, tissue compressibility in the LC, observed in ex vivo[35] and in situ[45] experiments, significantly affected the ONH strains. For instance, using the *Soft LC tissue parameter set* significantly diminished the decrease in strain magnitudes from reference to goggle configurations (see Fig. 5). Therefore, it is likely that the patients with different ONH biomechanics and glaucoma types would have some variability in the magnitude of ONH strain reduction for a given decrease in IOP due to NPP. For example, in pseudoexfoliation glaucoma (PEXG), LC stiffness is decreased,[46] whereas in primary open-angle glaucoma (POAG), the LC tends to stiffen.[2,47,48] Despite this variability, reducing IOP with NPP is still likely to be beneficial because ONH strains were decreased even at extreme LC stiffness and softness.

Although NPP decreased strain magnitudes in the ONH, it nonuniformly increased them in the cornea (<1% strain; see Figs. 2, 3). However, the increase in corneal strain induced by NPP was almost 4-fold smaller than the increase in corneal strain observed when IOP was increased from 15.6 mmHg to 31.6 mmHg (in the absence of Goggles; Hypertensive case; see Figs. 2, 3). Based on these findings, the observed increase in corneal strain due to NPP is estimated to be equivalent to that due to an IOP increase of c. 4 mmHg in a normotensive eye. For comparison, circadian changes in IOP have a similar magnitude,[49,50] and no adverse clinical effects are known to be caused by such physiological IOP variations. Additionally, although the role of corneal biomechanics in ocular pathophysiology remains an active area of vision science research, clinical experience indicates that the cornea tolerates high IOPs (c. 30 mmHg) relatively well, suggesting that strains equivalent to those due to an IOP increase of 4 mmHg would not cause significant sequelae in the cornea or angle. For example, Hjortdal demonstrated regional differences in meridional and circumferential strains in the human cornea produced by IOPs up to 100 mmHg.[51] Despite this significant amount of pressure loading and increase in the transcorneal pressure difference, no sign of damage was observed, which in collagenous soft tissues presents as a progressive decrease in tensile modulus.[52,53]

Further, several prospective clinical trials have examined the safety of NPP applied by the MPD system. A phase I trial exposed 30 eyes to an NPP of −15 mmHg for 30 minutes. No adverse events, including corneal events, were noted immediately following goggle removal and at 7 days post-intervention.[54] Similar safety outcomes were observed in a cohort of 65 healthy eyes treated with different amounts of NPP.[13] Additionally, no corneal adverse events were observed in glaucomatous eyes exposed to NPP overnight.[11,55] Clinical evidence corroborates existing corneal biomechanics research suggesting that the corneal strain induced by NPP is likely clinically insignificant.

A potential limitation of this study was the assumption that the IOP decrease due to NPP was unaffected by changing corneoscleral stiffness (see Fig. 4) and the spatial distribution of NPP (see Supplementary Fig. S4). In reality, we expect that corneoscleral stiffness and NPP distribution will modestly affect the magnitude of the IOP decrease; therefore, in the future, it would be worthwhile extending the model to include blood flow and fluid-solid interactions.[15] In addition, we focused on NPP's effect in normotensive eyes, because the clinical use scenario for the MPD system is primarily to treat glaucomatous eyes with progressive visual field loss despite medical therapy to lower IOP. However, our framework can be adapted to study cases with different baseline IOP levels. Further, for numerical efficiency, we assumed that the eye to be axisymmetric relative to its optical axis. In reality, the ONH axis is slightly off-center relative to the optical axis; however, this slight difference is unlikely to affect our results. In addition, we used simplified boundary conditions, which included the primary experimentally measured mechanical pressures (i.e., NPP, IOP, and RTLP), but not other effects, such as mechanical contact between the globe, the eyelids, and orbital structures.[56] The fidelity of the model could be improved by including such effects, but we suggest that such modifications are unlikely to affect the main conclusions since the primary driver of ocular response in our model was IOP, which we specified from experimental measurements. Further, experimental investigation of eyelid effect while using MPD showed that eyelids have a minimal impact on the IOP-lowering effect of NPP.[57] Finally, we assumed the extraocular rectus muscle/tendon to be a rigid body, and we did not consider the discrete attachment sites of the rectus muscles in the four anatomic quadrants (i.e., in our axisymmetric model, they were treated as a "band"

around the circumference of the eye). These simplifications are justified by the significantly higher stiffness of the rectus muscles and tendons relative to the other ocular tissues[58] and the insensitivity of our results to the specifics of the rectus muscle/tendon boundary conditions (see Supplementary Fig. S1).

In conclusion, this study provides novel insights into the biomechanical effects of NPP on the ONH and cornea. We showed that NPP decreases strain in ONH tissues by reducing IOP, whereas NPP increases cornea strains. The decrease of ONH strains is likely beneficial for glaucoma patients, whereas NPP-induced corneal strains are relatively small and likely clinically insignificant.

Acknowledgments

The authors thank our funding sources: the Georgia Research Alliance (CRE) and the BrightFocus Foundation (postdoctoral fellowship G2021005F, BNS).

Presented as conference abstracts at the 2022 Association for Research in Vision and Ophthalmology meeting, Denver, Colorado, and 2022 Summer Biomechanics Bioengineering and Biotransport Conference, Cambridge, Maryland.

Disclosure: **B.N. Safa**, None; **A. Bleeker**, None; **J.P. Berdahl**, Founder/CEO of Equinox Ophthalmic (the developer of the MPD system) and holds rights to intellectual property related to the MPD system; **C.R. Ethier**, Equinox Ophthalmic (C)

References

1. Sun Y, Chen A, Zou M, et al. Time trends, associations and prevalence of blindness and vision loss due to glaucoma: an analysis of observational data from the Global Burden of Disease Study 2017. *BMJ Open*. 2022;12:e053805.
2. Downs JC, Roberts MD, Burgoyne CF. Mechanical environment of the optic nerve head in glaucoma. *Optom Vis Sci*. 2008;85:425–435.
3. Safa BN, Wong CA, Ha J, Ethier CR. Glaucoma and biomechanics. *Curr Opin Ophthalmol*. 2022, https://doi.org/10.1097/ICU.0000000000000829.
4. Weinreb RN, Aung T, Medeiros FA. The Pathophysiology and Treatment of Glaucoma. *JAMA*. 2014;311:1901–1911.
5. Schuster AK, Erb C, Hoffmann EM, Dietlein T, Pfeiffer N. The Diagnosis and Treatment of Glaucoma. *Dtsch Arztebl Int*. 2020;117:225–234.
6. Heijl A, Leske MC, Bengtsson B, et al. Reduction of intraocular pressure and glaucoma progression: results from the Early Manifest Glaucoma Trial. *Arch Ophthalmol*. 2002;120:1268–1279.
7. Kim KE, Park K-H. Update on the Prevalence, Etiology, Diagnosis, and Monitoring of Normal-Tension Glaucoma. *Asia-Pacific J Ophthalmol*. 2016;5:23–31.
8. Agnifili L, Mastropasqua R, Frezzotti P, et al. Circadian intraocular pressure patterns in healthy subjects, primary open angle and normal tension glaucoma patients with a contact lens sensor. *Acta Ophthalmol*. 2015;93:e14–e21.
9. De Moraes CG, Jasien JV, Simon-Zoula S, Liebmann JM, Ritch R. Visual Field Change and 24-Hour IOP-Related Profile with a Contact Lens Sensor in Treated Glaucoma Patients. *Ophthalmology*. 2016;123:744–753.
10. Sheybani A, Scott R, Samuelson TW, et al. Open-Angle Glaucoma: Burden of Illness, Current Therapies, and the Management of Nocturnal IOP Variation. *Ophthalmol Ther*. 2020;9:1–14.
11. Goldberg JL, Jiminez-Roman J, Hernandez-Oteyza A, Quiroz-Mercado H. Short-term Evaluation of Negative Pressure Applied by the Multi-Pressure Dial System to Lower Nocturnal IOP: A Prospective, Controlled, Intra-subject Study. *Ophthalmol Ther*. 2021;10:349–358.
12. Samuelson TW, Ferguson TJ, Radcliffe NM, et al. 8 hrs Safety Evaluation Of A Multi-Pressure Dial In Eyes With Glaucoma: Prospective, Open-Label, Randomized Study. *Clin Ophthalmol*. 2019;13:1947–1953.
13. Swan RJ, Ferguson TJ, Shah M, et al. Evaluation of the IOP-Lowering Effect of a Multi-Pressure Dial at Different Negative Pressure Settings. *Transl Vis Sci Technol*. 2020;9:19.
14. Shafer B, Ferguson TJ, Chu N, Brambilla E, Yoo P. The Effect of Periocular Negative Pressure Application on Intraocular and Retrobulbar Pressure in Human Cadaver Eyes. *Ophthalmol Ther*. 2022;11:365–376.
15. Ethier CR, Yoo P, Berdahl JP. The effects of negative periocular pressure on intraocular pressure. *Exp Eye Res*. 2020;191:107928.
16. Boote C, Sigal IA, Grytz R, Hua Y, Nguyen TD, Girard MJA. Scleral structure and biomechanics. *Prog Retin Eye Res*. 2020;74:100773.
17. Feola AJ, Myers JG, Raykin J, et al. Finite Element Modeling of Factors Influencing Optic Nerve

Head Deformation Due to Intracranial Pressure. *Invest Ophthalmol Vis Sci*. 2016;57:1901–1911.
18. Girard MI. Scleral Biomechanics in the Normal, Glaucomatous Aging Eye. Tulane University; 2008.
19. Girard MJA, Downs JC, Burgoyne CF, Suh J-KKF. Peripapillary and posterior scleral mechanics - Part I: Development of an anisotropic hyperelastic constitutive model. *J Biomechan Engin*. 2009;131(5):051011.
20. Grytz R, Krishnan K, Whitley R, et al. A Mesh-Free Approach to Incorporate Complex Anisotropic and Heterogeneous Material Properties into Eye-Specific Finite Element Models. *Comput Methods Appl Mech Eng*. 2020;358: 112654.
21. Schwaner SA, Perry RN, Kight AM, et al. Individual-Specific Modeling of Rat Optic Nerve Head Biomechanics in Glaucoma. *J Biomech Eng*. 2021;143(4):041004.
22. Sigal IA, Flanagan JG, Ethier CR. Factors influencing optic nerve head biomechanics. *Invest Ophthalmol Vis Sci.* 2005;46:4189–4199.
23. Hernandez MR. The optic nerve head in glaucoma: role of astrocytes in tissue remodeling. *Prog in Retinal and Eye Res*. 2000;19:297–321.
24. Wallace DM, O'Brien CJ. The role of lamina cribrosa cells in optic nerve head fibrosis in glaucoma. *Exp Eye Res*. 2016;142:102–109.
25. Sigal IA, Flanagan JG, Tertinegg I, Ethier CR. Finite Element Modeling of Optic Nerve Head Biomechanics. *Invest Ophthalmol Vis Sci*. 2004;45:4378–4387.
26. Woo Y, Kobayashi AS, Lawrence C, Schlegel WA. Mathematical model of the corneo-scleral shell as applied to intraocular pressure-volume relations and applanation tonometry. *Ann Biomed Eng*. 1972;1:87–98.
27. Apt L. An anatomical reevaluation of rectus muscle insertions. *Trans Am Ophthalmol Soc*. 1980;78:365–375.
28. Geuzaine C, Remacle J-F. Gmsh: A 3-D finite element mesh generator with built-in pre- and post-processing facilities. *Int J Numerical Meth Eng*. 2009;79:1309–1331.
29. Schöberl J. NETGEN An advancing front 2D/3D-mesh generator based on abstract rules. *Comput Visual Sci*. 1997;1:41–52.
30. Maas SA, Ellis BJ, Ateshian GA, Weiss JA. FEBio: Finite Elements for Biomechanics. *J Biomechan Eng.* 2012;134:011005–011005.
31. Grytz R, Fazio MA, Girard MJA, et al. Material properties of the posterior human sclera. *J Mech Behav Biomed Mater*. 2014;29:602–617.
32. Battaglioli JL, Kamm RD. Measurements of the compressive properties of scleral tissue. *Invest Ophthalmol Vis Sci*. 1984;25:59–65.
33. Blackburn BJ, Jenkins MW, Rollins AM, Dupps WJ. A Review of Structural and Biomechanical Changes in the Cornea in Aging, Disease, and Photochemical Crosslinking. *Front Bioeng Biotechnol*. 2019;7:66.
34. Friberg TR, Lace JW. A comparison of the elastic properties of human choroid and sclera. *Exp Eye Res*. 1988;47:429–436.
35. Safa BN, Read AT, Ethier CR Assessment of the viscoelastic mechanical properties of the porcine optic nerve head using micromechanical testing and finite element modeling. *Acta Biomater*. 2021;134:379–387.
36. Bonet J, Wood RD, Nonlinear Continuum Mechanics for Finite Element Analysis. Second edition. Cambridge, UK: Cambridge University Press; 1997.
37. McEwen WK, Helen RS. Rheology of the Human Sclera. Unifying formulation of ocular rigidity. *Ophthalmol.* 1965;150:321–346.
38. Perrotta R. raaperrotta/symlog. 2022, https://github.com/raaperrotta/symlog. Accessed September 1, 2022.
39. Webber JBW. A bi-symmetric log transformation for wide-range data. *Meas Sci Technol.* 2012;24:027001.
40. Brusini P, Salvetat ML, Zeppieri M. How to Measure Intraocular Pressure: An Updated Review of Various Tonometers. *J Clin Med*. 2021;10:3860.
41. Berdahl JP, Allingham RR, Johnson DH. Cerebrospinal Fluid Pressure Is Decreased in Primary Open-angle Glaucoma. *Ophthalmology*. 2008;115:763–768.
42. Gordon MO, Beiser JA, Brandt JD, et al. The Ocular Hypertension Treatment Study: Baseline Factors That Predict the Onset of Primary Open-Angle Glaucoma. *Arch Ophthalmol*. 2002;120:714–720; discussion 829-830.
43. Chuangsuwanich T, Run TA, Braeu FA, et al. Differing Associations between Optic Nerve Head Strains and Visual Field Loss in Patients with Normal- and High-Tension Glaucoma. *Ophthalmology*. 2023;130:99–110.
44. Girard MJA, Beotra MR, Chin KS, et al. In Vivo 3-Dimensional Strain Mapping of the Optic Nerve Head Following Intraocular Pressure Lowering by Trabeculectomy. *Ophthalmology*. 2016;123:1190–1200.
45. Coudrillier B, Geraldes DM, Vo NT, et al. Phase-Contrast Micro-Computed Tomography Measurements of the Intraocular Pressure-Induced Defor-

mation of the Porcine Lamina Cribrosa. *IEEE Trans Med Imaging*. 2016;35:988–999.
46. Braunsmann C, Hammer CM, Rheinlaender J, Kruse FE, Schäffer TE, Schlätzer-Schrehardt U. Evaluation of Lamina Cribrosa and Peripapillary Sclera Stiffness in Pseudoexfoliation and Normal Eyes by Atomic Force Microscopy. *Invest Ophthalmol Vis Sci*. 2012;53:2960–2967.
47. Beotra MR, Wang X, Tun TA, et al. In Vivo Three-Dimensional Lamina Cribrosa Strains in Healthy, Ocular Hypertensive, and Glaucoma Eyes Following Acute Intraocular Pressure Elevation. *Invest Ophthalmol Vis Sci*. 2018;59:260–272.
48. Hommer A, Fuchsjäger-Mayrl G, Resch H, Vass C, Garhofer G, Schmetterer L. Estimation of Ocular Rigidity Based on Measurement of Pulse Amplitude Using Pneumotonometry and Fundus Pulse Using Laser Interferometry in Glaucoma. *Invest Ophthalmol Vis Sci*. 2008;49:4046–4050.
49. Barkana Y, Anis S, Liebmann J, Tello C, Ritch R. Clinical utility of intraocular pressure monitoring outside of normal office hours in patients with glaucoma. *Arch Ophthalmol*. 2006;124:793–797.
50. Hughes E, Spry P, Diamond J. 24-hour monitoring of intraocular pressure in glaucoma management: a retrospective review. *J Glaucoma*. 2003;12:232–236.
51. Hjortdal JØ. Regional elastic performance of the human cornea. *J Biomech*. 1996;29:931–942.
52. Safa BN, Lee AH, Santare MH, Elliott DM. Evaluating Plastic Deformation and Damage as Potential Mechanisms for Tendon Inelasticity Using a Reactive Modeling Framework. *J Biomech Engin*. 2019;141:101008.
53. Zitnay JL, Li Y, Qin Z, et al. Molecular level detection and localization of mechanical damage in collagen enabled by collagen hybridizing peptides. *Nat Commun*. 2017;8:14913.
54. Thompson VM, Ferguson TJ, Akmed IIK, et al. Short-Term Safety Evaluation of a Multi-Pressure Dial: A Prospective, Open-label, Non-randomized Study. *Ophthalmol Ther*. 2019;8:279–287.
55. Ferguson TJ, Radcliffe NM, Van Tassel SH, et al. Overnight Safety Evaluation of a Multi-Pressure Dial in Eyes with Glaucoma: Prospective, Open-Label, Randomized Study. *Clin Ophthalmol*. 2020;14, 2739–2746.
56. Sakai E, Shiraishi A, Yamaguchi M, Ohta K, Ohashi Y. Blepharo-tensiometer: new eyelid pressure measurement system using tactile pressure sensor. *Eye Contact Lens*. 2012;38:326–330.
57. Chu N, Brambilla E, Yoo P, Ferguson TJ. Evaluation of negative pressure transfer through tissue in a benchtop cornea and eyelid model. *Ther Adv Ophthalmol*. 2020;12:2515841420971406.
58. Yoo L, Reed J, Shin A, Demer JL. Atomic force microscopy determination of Young's modulus of bovine extra-ocular tendon fiber bundles. *J Biomech*. 2014;47:1899–1903.
59. Weiss JA, Maker BN, Govindjee S. Finite element implementation of incompressible, transversely isotropic hyperelasticity. *Computer Methods Appl Mech Engin*. 1996;135: 107–128.
60. Maas S, Weiss J, Ateshian G. FEBio User's Manual 3.5. 2021. Available at: https://help.febio.org/FebioUser/FEBio_um_3-4.html. Accessed August 30, 2021
61. Jesus DA, Kedzia R, Iskander DR. Precise measurement of scleral radius using anterior eye profilometry. *Contact Lens and Anterior Eye*. 2017;40:47–52.
62. Medeiros FA, Sample PA, Weinreb RN. Corneal thickness measurements and visual function abnormalities in ocular hypertensive patients. *Am J Ophthalmol*. 2003;135:131–137.

Appendix: Constitutive Equations

Tissues were treated as incompressible neo-Hookean materials described by the following constitutive equation:

$$\Psi_{NH} = \frac{E}{6}\left(\tilde{I}_1 - 3\right) + \frac{K}{2} ln(J)^2 \qquad \text{(A1)}$$

where $\tilde{I}_1$ is the first invariant of the deviatoric right Cauchy-Green strain tensor ($\tilde{\mathbf{C}}$); J is the Jacobian of the deformation, $J = \det(\mathbf{F})$ with $\mathbf{F}$ being the deformation gradient tensor; E is the Young's modulus; and K is the bulk modulus. The values of E were taken from the literature (Table 2). When specifying K, we note that the material incompressibility constraint (i.e., $J = 1$), nominally eliminates the effect of K on material behavior; however, K is used as a penalty factor to enforce incompressibility, and it was set as a large value relative to E.[59]

We implemented the effects of collagen fibers in the ppSC using an equation suitable for the uncoupled nearly incompressible formulation (modified from *fiber-pow-linear-uncoupled material*[60]):

$$\tilde{\Psi}_f = \begin{cases} 0 & \tilde{I}_f \le 1 \\ \frac{1}{2}E_f\left(\tilde{I}_f - 1\right) - E_f\left(\sqrt{\tilde{I}_f} - 1\right) & 1 < \tilde{I}_f \end{cases} \qquad \text{(A2)}$$

where E_f is the fiber Young's modulus, and $\tilde{I}_f$ is the square of fiber stretch, calculated as $\tilde{I}_f = \boldsymbol{n}_f.\tilde{\mathbf{C}}.\boldsymbol{n}_f$, where $\boldsymbol{n}_f$ is the unit vector defining the fiber orientation.